Phase Diagrams of Self-Assembled Mono-Tethered Nanospheres from Molecular Simulation and Comparison to Surfactants

Christopher R. Iacovella,[†] Mark A. Horsch,[†] Zhenli Zhang,[†] and Sharon C. Glotzer*[,†,‡]

Departments of Chemical Engineering and Materials Science & Engineering, University of Michigan, Ann Arbor, Michigan 48109-2136

Received April 18, 2005. In Final Form: June 27, 2005

We perform Brownian dynamics simulations on model 3-D systems of mono-tethered nanospheres (TNS) to study the equilibrium morphologies formed by their self-assembly in a selective solvent. We predict that in contrast to flexible amphiphiles the nanospheres are locally ordered and there is an increase in the local order with an increase in concentration or relative nanoparticle diameter. We present the temperature vs concentration phase diagram for a system of TNS and propose a dimensionless scaling factor F_v (headgroup volume/tether volume) that allows a comparison between the morphologies formed from TNS and traditional surfactants.

I. Introduction

An impressive variety of nanoparticles of different materials and geometries has been synthesized[1], including but not limited to Au nanospheres,[2−7] Ag nanocubes and polyhedra,[8−10] $Al(OH)_3$ platelets,[11,12] Ag[5,13] and Au[14] triangles, and so forth.[1,15,16] This vast library of nanoparticles will provide the building blocks for tomorrow's materials,[17] if they can be assembled from the "bottom up" into ordered arrays. Bottom-up assembly provides an unprecedented number of opportunities for engineering novel materials with specific physical properties. However, the size scale and potentially large number of nanoparticles required to assemble macroscopic materials precludes mechanical methods as viable means for bottom-up assembly. Self-assembly is generally regarded as a promising means to reliably facilitate the assembly of large numbers of nano-building blocks (NBBs) into desirable structures,[18] but a predictive theory of assembled phases for nanoparticle systems is not yet in hand.

Functionalization of nanoparticles with a small number of oligomeric or polymeric tethers[19] is a novel strategy to induce the self-assembly of NBBs in a predictable and controllable manner. In this scheme, thermodynamic immiscibility between nanoparticle and tether, induced by temperature, concentration, or solvent selectivity, facilitates assembly, and the building block topology and nanoparticle shape influence the structure formed by the self-assembly process.[19] To this extent, recent advances in synthesis techniques are providing ever-increasing control over the size and shape of nanoparticles, and it is now possible to attach a small number of polymer tethers to specific locations on the surface of the nanoparticles,[3,20−27] creating "shape amphiphiles[28]" with controlled topology. For example, Westenhoff and Kotov attached a single tether to the surface of a CdTe quantum dot;[24] Alivisatos and co-workers demonstrated their ability to attach one, two, three, or more tethers to the surface of spherical, Au nanoparticles;[29] Stellacci and co-workers developed a technique that allows them to pattern the surface of spherical, Au nanoparticles with rings of tethers.[2] These

* To whom correspondence should be addressed. E:mail: sglotzer@umich.edu.
[†] Department of Chemical Engineering.
[‡] Department of Materials Science & Engineering.

(1) Murray, C. B.; Kagan, C. R.; Bawendi, M. G. *Ann. Rev. Mater. Sci.* **2000**, *30*, 545−610.
(2) Jackson, A. M.; Myerson, J. W.; Stellacci, F. *Nat. Mater.* **2004**, *3*, 330−336.
(3) Li, Z.; Jin, R. C.; Mirkin, C. A.; Letsinger, R. L. *Nucl. Acids Res.* **2002**, *30*, 1558−1562.
(4) Yang, J.; Lee, J. Y.; Deivaraj, T. C.; Too, H. P. *J. Colloid Interface Sci.* **2004**, *277*, 95−99.
(5) Sun, Y. G.; Xia, Y. N. *Analyst* **2003**, *128*, 686−691.
(6) Daniel, M. C.; Astruc, D. *Chem. Rev.* **2004**, *104*, 293−346.
(7) Sakai, T.; Alexandridis, P. *Langmuir* **2004**, *20*, 8426−8430.
(8) Wiley: B.; Sun, Y. G.; Mayers, B.; Xia, Y. N. *Chem. Eur. J.* **2005**, *11*, 454−463.
(9) Im, S. H.; Lee, Y. T.; Wiley: B.; Xia, Y. *Angew. Chem. Int. Ed.* **2005**, *44*, 2154−2157.
(10) Sun, Y. G.; Xia, Y. N. *Science* **2002**, *298*, 2176−2179.
(11) van der Beek, D.; Lekkerkerker, H. N. W. *Europhys. Lett.* **2003**, *61*, 702−707.
(12) van der Kooij, F. M.; Kassapidou, K.; Lekkerkerker, H. N. W. *Nature* **2000**, *406*, 868−871.
(13) Jin, R. C.; Cao, Y. W.; Mirkin, C. A.; Kelly, K. L.; Schatz, G. C.; Zheng, J. G. *Science* **2001**, *294*, 1901−1903.
(14) Malikova, N.; Pastoriza-Santos, I.; Schierhorn, M.; Kotov, N. A.; Liz-Marzan, L. M. *Langmuir* **2002**, *18*, 3694−3697.
(15) Ohno, T.; Yatsuya, S. *J. Mater. Sci.* **1998**, *33*, 5843−5847.
(16) Manna, L.; Milliron, D. J.; Meisel, A.; Scher, E. C.; Alivisatos, A. P. *Nat. Mater.* **2003**, *2*, 382−385.
(17) Glotzer, S. C.; Solomon, M. J.; Kotov, N. A. *AIChE J.* **2004**, *50*.
(18) Whitesides, G. M.; Grzybowski, B. *Science* **2002**, *295*, 2418−2421.
(19) Zhang, Z.-L.; Horsch, M. A.; Lamm, M. H.; Glotzer, S. C. *Nano Lett.* **2003**, *3*, 1341−1346.
(20) Tokareva, I.; Hutter, E. *J. Am. Chem. Soc.* **2004**, *126*, 15784−15789.
(21) Storhofff, J. J.; Elghanian, R.; Mirkin, C. A.; Letsinger, R. L. *Langmuir* **2002**, *18*, 6666−6670.
(22) Song, T.; Dai, S.; Tam, K. C.; Lee, S. Y.; Goh, S. H. *Polymer* **2003**, *44*, 2529−2536.
(23) Song, T.; Dai, S.; Tam, K. C.; Lee, S. Y.; Goh, S. H. *Langmuir* **2003**, *19*, 4798−4803.
(24) Westenhoff, S.; Kotov, N. A. *J. Am. Chem. Soc.* **2002**, *124*, 2448−2449.
(25) Park, S.; Brown, K. A.; Hamad-Schifferli, K. *Nano Lett.* **2004**, *4*, 1925−1929.
(26) Park, S. J.; Lazarides, A. A.; Storhoff, J. J.; Pesce, L.; Mirkin, C. A. *J. Phys. Chem. B* **2004**, *108*, 12375−12380.
(27) Sung, K. M.; Mosley, D. W.; Peelle, B. R.; Zhang, S. G.; Jacobson, J. M. *J. Am. Chem. Soc.* **2004**, *126*, 5064−5065.
(28) Glotzer, S. C. *Science* **2004**, *306*, 419−420.
(29) Parak, W. J.; Pellegrino, T.; Micheel, C. M.; Gerion, D.; Williams, S. C.; Alivisatos, A. P. *Nano Letters* **2003**, *3*, 33−36.

10.1021/la051035l CCC: $30.25
Published on Web 09/15/2005

and other tethered nanoparticles[30] serve as a proof of concept and represent substantial progress toward realizing NBBs with specific geometry and topology. It may be expected that shape amphiphiles will self-assemble into microphases similar to those observed in block copolymers (BCP) and surfactants and that the underlying self-assembly process is governed by similar physics, whereby systems seek to minimize their free energy through aggregation of like species. One distinct difference between tethered NBBs and BCPs and surfactants is that the "head" groups of the NBBs are rigid, resulting in a large excluded volume for which the effects on the self-assembly process are unclear. The overall concentration-dependent phase behavior of surfactant solutions has been studied computationally via lattice and off-lattice Monte Carlo (MC),[31,32] most notably by Larson.[33,34] Computational studies of surfactants using molecular and Brownian dynamics methods have thus far been limited to small regions of the phase diagram.[35−43] Recently, Bourov and Bhattacharya studied a two- and three-dimensional system of surfactants with large headgroups.[37,38] In their study, they used a model and method similar to that proposed by Zhang et al.,[19] where the surfactant was modeled as a large spherical particle permanently bonded to a flexible chain. They showed the impact of headgroup size on the critical micelle concentration was commensurate with experimental predictions. Since their work was limited to the study of micelles[37,38] the effects of a large rigid headgroup on other phases was not reported. We report such effects here.

In this paper, we investigate the simplest of the nanoparticle geometries and topologies to use as a datum for future studies of tethered nanoparticle shape amphiphiles as well as to compare with surfactants. In particular, we are interested in the extent to which a tethered nanosphere behaves like a traditional surfactant molecule at least qualitatively. To this end, we have developed a model building block for mono-tethered nanospheres (TNS) and perform Brownian dynamics (BD) simulations to investigate the tendency for these model NBBs to self-assemble. We examine a wide range of concentrations that allow the study of a range of self-assembled morphologies. To investigate the extent to which TNS are similar to surfactants and to provide a direct comparison between the TNS and the flexible chain model developed by Larson,[33] we study both the TNS model and a modified Larson model with BD. Through comparison between these two models, we ascertain the effects of the large rigid headgroup as it pertains to self-assembled phases.

II. Model/Method

In this work, we aim to predict the assembled structures formed from TNS. Because of the wide variety of materials nanoparticles can be synthesized from, coated with, and tethered to, it is challenging to develop a model that will be generally applicable for all cases. To resolve this issue, we have focused our coarse-grained model on three key factors necessary in the study of any tethered nanoparticle shape amphiphile: (1) nanoparticle geometry, (2) tether and tethered nanoparticle topology, and (3) amphiphilicity. To allow for the realization of longer time scales and large systems, BD is utilized. As shown by von Gottberg et al.,[35,36] BD is capable of capturing the appropriate details of the simulations for surfactants, while making the simulations less computationally expensive. BD is a subset of Langevin dynamics wherein the particle trajectories are governed by the Langevin equation.

$$m_i \frac{dv_i(t)}{dt} = -\gamma_i v_i(t) + F_i\{x(t)\} + R_i(t) \quad (1)$$

The left-hand side of eq 1 is the force felt by particle i at time t. The first term on the right-hand side is the nonconservative drag force, F_i is the deterministic force obtained from differentiation of the conservative potential field, and R_i is the stochastic force, which satisfies the fluctuation dissipation theorem. The variable γ_i is the friction coefficient and is related to solvent viscosity η by Stoke's equation

$$\gamma_i = 6\pi\eta a = k_B T/D \quad (2)$$

where "a" is the radius of the solute particle (here, a tether or headgroup bead, defined below), k_B is Boltzmann's constant, T is the temperature, and D is the diffusion coefficient. In BD, solvent molecules are treated implicitly in a statistical manner, which significantly reduces the number of force calculations required. In this study, it is assumed that the solvent molecules are small as compared to the nanoparticles such that they are space-filling. This assumption is supported by the characteristic diameter of two commonly used solvents, water and tetrahydrofuran, with characteristic diameters of ∼0.3 nm[44] and ∼0.5 nm[45] respectively. Since the solvent molecules are considerably smaller than the nano-building blocks, implicit treatment of the solvent also avoids resolving the time scale necessary to consider them. Additionally, the dissipative forces in the BD method increase the allowable time steps for integrating the equations of motion.

To capture the amphiphilic nature of tethered nanospheres and to avoid limiting our studies to a specific type of nanoparticle, we implement empirical pair potentials that have been successful in the study of BCPs and surfactants. These pair potentials that act between each component of the NBB effectively model the solvent-phobic/solvent-philic interactions expected of tethered nanoparticles, where the solvent may interact with the bare particle or with stabilizers that coat the nanoparticle[2]. Following Zhang et al.[19] nanospheres are modeled as spheres of diameter "d", permanently connected to tethers via finitely extensible nonlinear elastic (FENE) springs

$$U_{ij}^{FENE}(r) = -\frac{1}{2}kR_0^2 \ln\left[1 - \left(\frac{r_{ij}}{R_0}\right)^2\right] \quad (3)$$

where R_0 is the maximum allowable separation, and k is the spring constant. Tethers are modeled as chains of beads of diameter σ connected via FENE springs (eq 3).

Amphiphilicity is modeled by treating tether beads and nanoparticles with different potentials. In all cases, we study

(30) Lu, X. M.; Hanrath, T.; Johnston, K. P.; Korgel, B. A. *Nano Lett.* **2003**, *3*, 93−99.
(31) Siperstein, F. R.; Gubbins, K. E. *Langmuir* **2003**, *19*, 2049−2057.
(32) Lisal, M.; Hall, C. K.; Gubbins, K. E.; Panagiotopoulos, A. Z. *Mol. Simul.* **2003**, *29*, 139−157.
(33) Larson, R. G. *J. Phys. II* **1996**, *6*, 1441−1463.
(34) Larson, R. G. *Chem. Eng. Sci.* **1994**, *49*, 2833−2850.
(35) von Gottberg, F. K.; Smith, K. A.; Hatton, T. A. *J. Chem. Phys.* **1998**, *108*, 2232−2244.
(36) von Gottberg, F. K.; Smith, K. A.; Hatton, T. A. *J. Chem. Phys.* **1997**, *106*, 9850−9857.
(37) Bourov, G. K.; Bhattacharya, A. *J. Chem. Phys.* **2003**, *119*, 9219−9225.
(38) Bourov, G. K.; Bhattacharya, A. *J. Chem. Phys.* **2005**, *122*.
(39) Loison, C.; Mareschal, M.; Schmid, F. *J. Chem. Phys.* **2004**, *121*, 1890−1900.
(40) Loison, C.; Mareschal, M.; Kremer, K.; Schmid, F. *J. Chem. Phys.* **2003**, *119*, 13138−13148.
(41) Soddemann, T.; Dunweg, B.; Kremer, K. *Eur. Phys. J. E* **2001**, *6*, 409−419.
(42) Fodi, B.; Hentschke, R. *Langmuir* **2000**, *16*, 1626−1633.
(43) Salaniwal, S.; Cui, S. T.; Cochran, H. D.; Cummings, P. T. *Langmuir* **2001**, *17*, 1773−1783.
(44) Berendsen, H. J. C.; Grigera, J. R.; Straatsma, T. P. *J. Phys. Chem.* **1987**, *91*, 6269−6271.
(45) Meyer, H.; Biermann, O.; Faller, R.; Reith, D.; Muller-Plathe, F. *J. Chem. Phys.* **2000**, *113*, 6264−6275.

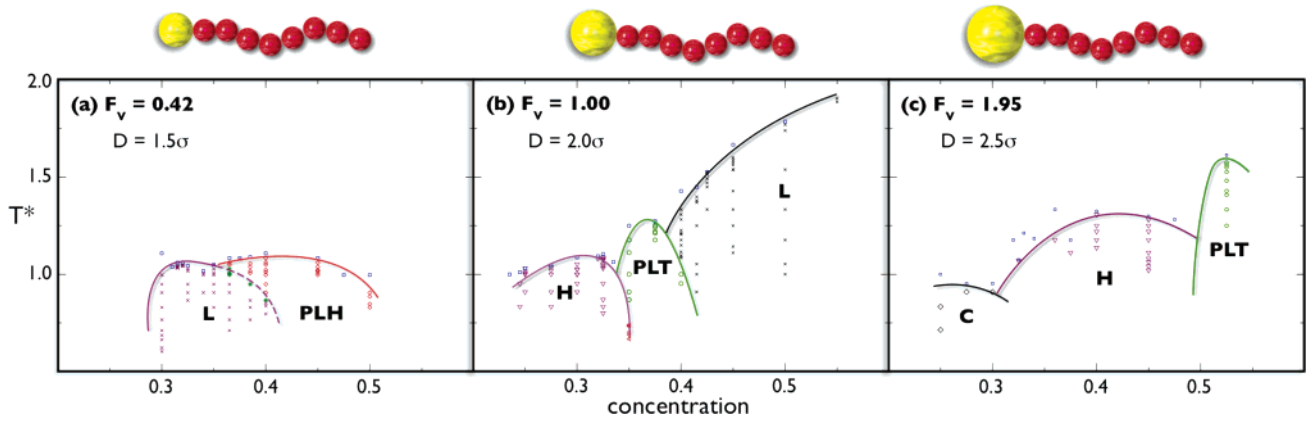

Figure 1. Temperature vs concentration phase diagrams for h1t8 TNS systems, with schematic representations of simulated TNS displayed above diagrams. Data points indicate performed runs. Phases are defined as lamellae (L), perforated lamellae through the headgroup (PLH), hexagonally packed cylinders (H), perforated lamellae through tethers (PLT), cubic ordered spherical micelles (C). (a) Phase diagram for TNS with particle diameter $d = 1.5\sigma$, (b) particle diameter $d = 2.0\sigma$, (c) particle diameter $d = 2.5\sigma$. In (a−c), the phase boundaries are approximate and drawn as guides for the eye.

tethers (or tails in surfactants) that are solvent-phobic; to model solvent-phobic conditions, like species interact via a shifted Lennard−Jones potential

$$\begin{cases} U_{ij}^{\mathrm{LJ}}(r) = 4\epsilon_{ij}\left[\left(\frac{\sigma}{r_{ij}}\right)^{12} - \left(\frac{\sigma}{r_{ij}}\right)^{6}\right] + U_{ij}^{\mathrm{LJ}}(r_c) & r < r_c \\ U_{ij}^{\mathrm{LJ}}(r) = 0 & r \geq r_c \end{cases} \quad (4)$$

whereby there is a relatively short-range attraction between the particles. This effectively models both the excluded volume and the desire of the tethers to minimize solvent contact and thus aggregate. Species of different type interact via a purely repulsive Weeks−Chandler−Anderson (WCA) soft-sphere potential

$$\begin{cases} U_{ij}^{\mathrm{WCA}}(r) = 4\epsilon_{ij}\left[\left(\frac{\sigma}{r_{ij} - \alpha}\right)^{12} - \left(\frac{\sigma}{r_{ij} - \alpha}\right)^{6}\right] + \epsilon_{ij} & r < r_c \\ U_{ij}^{\mathrm{WCA}}(r) = 0 & r \geq r_c \end{cases} \quad (5)$$

to account for excluded volume interactions. Nanoparticles (and surfactant headgroups) are treated as being solvent-philic and are modeled with a WCA potential to avoid enthalpically driven aggregation. Note that we shift the WCA potential to the surface of the nanoparticle by use of the variable α. The degree of immiscibility is determined by the reciprocal temperature, ϵ/k_BT, where ϵ is the potential well depth.

All simulations are performed in a cubic simulation box. Systems are slowly quenched from a high-temperature disordered state to a target temperature. System sizes are varied from $N = 8000$ to $N = 45\,000$, where N is the number of beads in the system. The natural units of these systems are σ and ϵ and the dimensionless time is $t^* = \sigma\sqrt{m/\epsilon}$, where m is the mass of a tether bead, σ is the diameter of a tether bead, and ϵ is the interaction parameter. In all cases, concentration, ϕ, is defined as the ratio of excluded volume of the beads to the system volume, and dimensionless temperature, T^*, is defined as k_BT/ϵ. The stress tensor is monitored to ensure that the systems are neither compressed nor stretched.[46] Also, the periodic spacing in the self-assembled structures and the energy per particle are compared for the different system sizes to ensure any finite size effects are avoided.

III. Results/Discussion

To explore the impact of nanoparticle diameter on the overall phase behavior of TNS, we have conducted a series of studies where the length of the bead-spring tether is fixed and the nanoparticle diameter is varied. Simulations are performed for a tether length of 8 beads of diameter σ and nanoparticle diameters of $d = 1.5\sigma$, 2.0σ, and 2.5σ. For direct comparison to surfactant systems, we also study flexible chains of two head beads (h2t8) and eight head beads (h8t8) all with tether length of 8 beads. We present a temperature vs concentration phase diagram for a three-dimensional system of TNS and compare the TNS phase diagram to that of surfactants. We further present a "phase diagram" given by a scaling factor, (F_v) = (headgroup volume/tether volume), plotted versus concentration. We predict the existence of three distinct regimes in the phase behavior of TNS. The first regime is where the headgroup volume is small compared to the tether volume and lamellar phases are predominant, the second regime is where headgroup and tether volumes are similar, resulting in a rich combination of phases, and the third is where the headgroup volume is larger than the tether volume and phases with a high degree of curvature are dominant.

III.1. Nanoparticle Volume Smaller than Tether Volume. We predict for TNS with a nanoparticle diameter of $d = 1.5\sigma$ and a fully extended tether length of 8σ that the equilibrium structures are limited to sheetlike (lamellar) structures over a wide range of concentrations, $\phi \approx 0.3-0.5$, as shown in the phase diagram presented in Figure 1a. For $\phi \approx 0.3-0.35$, we observe the formation of lamellar (L) sheets for temperatures below the order−disorder temperature, T_{ODT}. For $\phi \approx 0.35-0.4$, we observe the formation of a perforated lamellar phase (PLH) for higher temperatures and the formation of a lamellar phase for lower temperatures provided $T < T_{\mathrm{ODT}}$. For $\phi \approx 0.4-0.5$, we predict only the PLH phase; an example simulation snapshot is shown in Figure 2a,b. The PLH phase observed for the higher concentrations is limited to perforations through the layer formed by the headgroup; in contrast, the perforated lamella through the tether region (PLT)—the inverse of the PLH phase—is typically reported for surfactant systems. For concentrations outside those discussed above the system is either disordered or composed of disordered micelles.

III.2. Nanoparticle Volume as Large as Tether Volume. For a nanoparticle diameter of $d = 2.0\sigma$ connected to a tether with a fully extended length of 8σ, we observe the formation of hexagonally packed cylinders (H), lamellae (L), and perforated lamellae (PLT), where the perforations are through the tether layers, as shown in the phase diagram presented in Figure 1b. For $\phi \approx 0.25-0.35$, we observe the formation of the H phase (a simulation snapshot is shown in Figure 3a), for intermediate $\phi \approx 0.35-0.4$, we observe the PLT phase, and for $\phi \approx 0.4-0.55$, we observe the L phase (a simulation

(46) Cui, S. T.; Cummings, P. T.; Cochran, H. D. *Mol. Phys.* **1996**, *88*, 1657−1664.

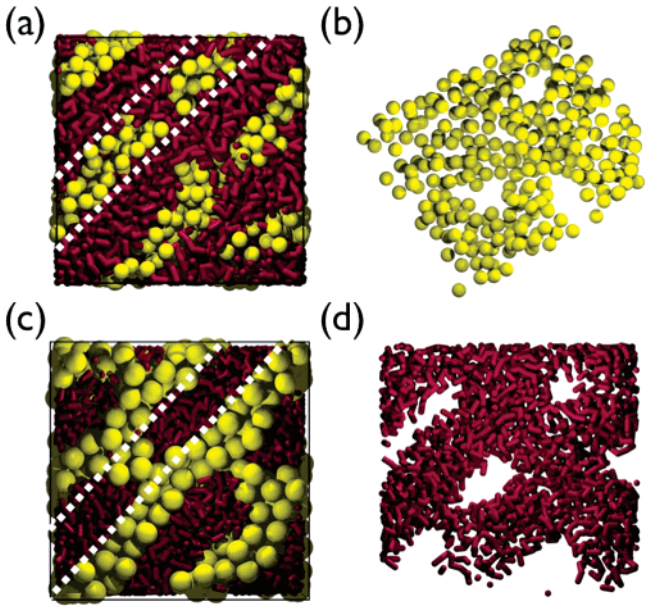

Figure 2. (a) Perforated lamella through the heads (PLH) for $d = 1.5\sigma$, $\phi = 0.45$, $T^* = 1.0$. (b) A single sheet showing perforations as dotted in (a). (c) Perforated lamella through the tethers (PLT) for $d = 2.5\sigma$, $\phi = 0.525$, $T^* = 1.5$. (d) A single sheet showing perforations as dotted in (c).

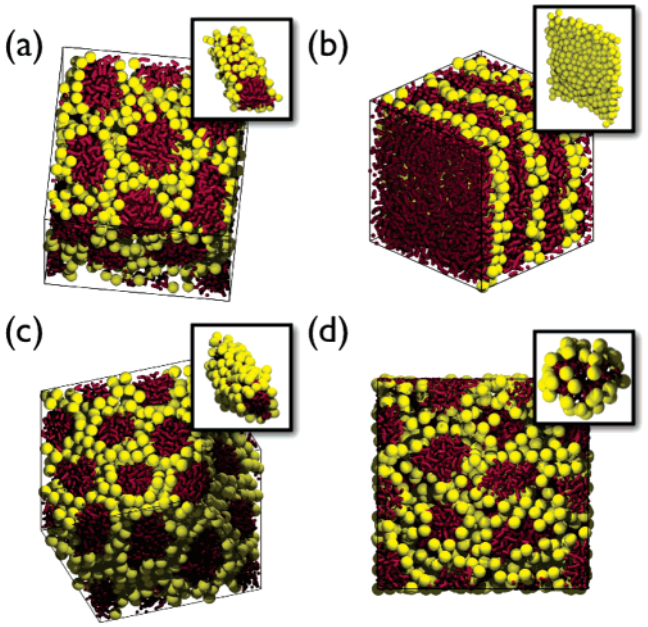

Figure 3. (a) Hexagonally packed cylinders (H) for $d = 2.0\sigma$, $\phi = 0.3$, $T^* = 1.0$. (b) Lamellar bilayers (L) for $d = 2.0\sigma$, $\phi = 0.55$, $T^* = 1.8$. (c) Hexagonally packed cylinders (H) for $d = 2.5\sigma$, $\phi = 0.45$, $T^* = 1.25$. (d) Cubic ordered micelles for $d = 2.5\sigma$, $\phi = 0.275$, $T^* = 1.2$.

snapshot is shown in Figure 3b). Here the volume of the headgroup is equivalent to the volume of the tether and for most of the phase diagram sheetlike structures are favored. However, in contrast to the case with the small headgroup we observe the formation of a structure with a curved interface, the H phase, at lower concentrations.

III.3. Nanoparticle Volume Larger than Tether Volume. For a nanoparticle diameter $d = 2.5\sigma$ connected to a tether with a fully extended length of 8σ, we observe the formation of cubic micelles (C), hexagonally packed cylinders (H), lamellae (L), and perforated lamellae (PLT), where the perforations are through the tether layers, as shown in the phase diagram presented in Figure 1c. For

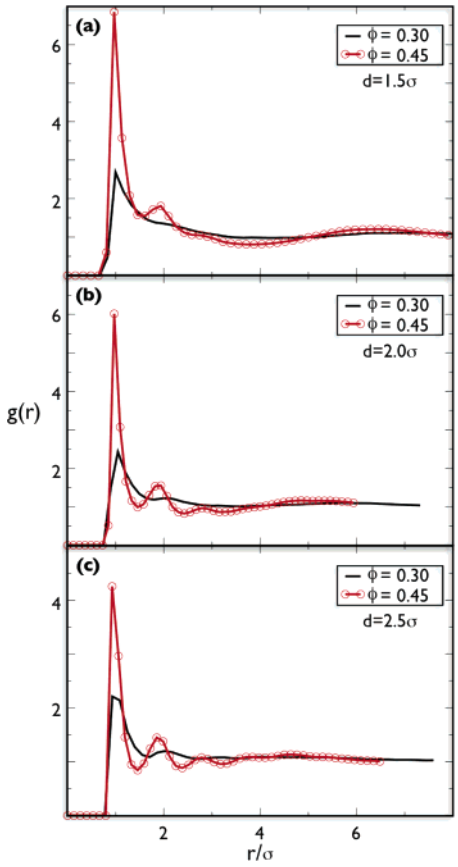

Figure 4. (a) Radial distribution function, $g(r)$, calculated for nanoparticles (headgroups) center-to-center, for $d = 1.5\sigma$, $\phi = 0.3$ and $\phi = 0.45$, $T^* = 1.0$. (b) $g(r)$ for $d = 2.0\sigma$, $\phi = 0.3$ and $\phi = 0.45$, $T^* = 1.0$. (c) $g(r)$ for $d = 2.5\sigma$, $\phi = 0.3$ and $\phi = 0.45$, $T^* = 1.0$.

this case, the headgroup volume is larger than the tether volume and we observe the formation of an additional structure with a curved interface, cubically ordered spherical micelles (C). A simulation snapshot of the cubically ordered spherical micelle phase is shown in Figure 3d. We further observe that structures with curved interfaces now dominate the majority of the phase diagram and that the only sheetlike phase is limited to the PLT phase; simulation snapshots of the PLT phase are shown in Figure 2c,d. Here, the H phase, shown in Figure 3c, is stabilized over a broad range of concentrations as compared to smaller headgroups. As headgroup diameter is further increased to 3.0σ, this trend toward structures with curved interfaces continues and the phase behavior is primarily limited to spherical micelles.

We observe that as the nanoparticle increases in size relative to the size of the tether, sheetlike structures are destabilized while structures with curved interfaces are stabilized. The limiting case of TNS with a relatively small nanoparticle is restricted to sheetlike structures, while the limiting case of a TNS with a relatively large headgroup is restricted to structures with curved interfaces. For intermediate cases, the phase diagram exhibits a combination of curved and sheetlike structures. In all cases of nanoparticle size, we predict an increase in the ordering of the nanoparticles (headgroups) with an increase in concentration of the system; this trend is shown by the number and intensity of peaks of the radial distribution function as concentrations of 0.3 and 0.45 are compared in Figure 4. As the system concentration is increased, the structures tend toward sheetlike structures where the nanoparticles arrange themselves within the sheets into

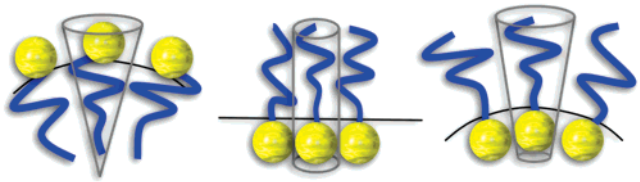

Figure 5. Depiction of the impact of interface curvature on the effective volume for tethered nanoparticles in three example mesophases observed.

hexagonal patterns, the most efficient packing of spheres in two-dimensions. Additionally, we predict that as particle diameter is increased, the temperature at which ordered phases form increases for a given mesophase, as can be seen by comparing the phase diagrams represented in Figure 1.

III.4. Perforated Lamella Phase. Perforated lamellae have been observed for surfactants both computationally[47,48] and experimentally[49,50] at concentrations very close to where the gyroid phase is observed.[33,49,51] This phase can be understood as arising from a competition between the formation of curved interfaces and planar interfaces. For large nanoparticles, as concentration is increased from low to high, there is a tendency for the interface curvature to decrease; however, this behavior is to some extent mitigated by the desire of the tails to maintain maximum contact, resulting in the PLT phase (a simulation snapshot is shown in Figure 2c,d). Conversely, for small nanoparticles increasing concentration tends to induce inverted interface curvature because now the tails stretch, decreasing the effective grafting density of the tethers, and resulting in the PLH phase (a simulation snapshot is shown in Figure 2a,b). This interface behavior is illustrated in Figure 5.

III.5. Packing Factor Analysis. This phase behavior can, in part, be rationalized by examining the packing factor, S, developed for surfactant systems.[52] The packing factor is a purely geometric argument as to why certain structures form in surfactants. The geometry of associated structures depends on "packing" properties of the amphiphile: the optimal area of the headgroup, a_o, volume of the chain, V, and the critical length of the tether, l_c .

$$S = \frac{V}{a_o l_c} \tag{6}$$

The packing factor S, effectively a dimensionless volume, relates the actual volume occupied by the tail to the ideal volume that would be occupied if the interface were planar. It is reasonable to assume and we observe that with a fixed tether length, the effective tether volume and length remain roughly constant regardless of head size, for the range of sizes studied. The effective area depends on the square of the diameter of the headgroup; therefore, large diameters result in a large a_o and S decreases with the square of the diameter of the headgroup. On the basis of the arguments given by Israelachvili, represented in Table 1, curved structures are favored for large headgroups.

Table 1. Values of the Israelachvili Packing Factor, *S*, and the Expected Structure[a]

S	structure
$S < 1/3$	spherical micelles
$1/3 < S < 1/2$	cylindrical micelles
$1/2 < S < 1$	flexible bilayers
$S \approx 1$	planar bilayers
$S > 1$	inverted micelles

[a] Adapted from ref 52.

Conversely, if the diameter is small, a_o is small, and therefore S is large, favoring sheetlike and inverted structures.

The Israelachvili packing factor can also help to explain the specific transitions we see regarding the perforated lamella phases. Starting from the H phase, increasing the concentration requires the headgroups to pack more densely, resulting in a decrease in a_o and consequently an increase in S, favoring sheetlike structures over curved ones. If instead we start with the L phase at low concentration and subsequently increase the concentration, a_o will again decrease, favoring structures with inverted curvature.

III.6. Comparison to Surfactants. Since measurements of the various quantities in S are often difficult to determine, especially when trying to compare a rigid sphere to a chain, a relationship that includes easily determinable quantities is needed to allow for direct comparison between a variety of different systems. We first discuss the comparison of the flexible headgroup surfactant to the TNS. We obtain the phase behavior of a symmetric h8t8 surfactant system using our modified Larson model, where both head and tail beads are modeled as flexible chains, connected by FENE springs within a BD simulation. In the standard Larson model, a surfactant is modeled by i "head" units connected to j "tail" units, where each unit occupies a site on a simple cubic lattice.[33] We find remarkable agreement with the phase diagrams plotted by Larson for h4t4 symmetric surfactant systems[33] as well as with the phase behavior mapped by Prinsen et al. using dissipative particle dynamics (DPD).[53] Figure 6a shows the h2t8 surfactant phase diagram, Figure 6b shows the phase diagram for a system of TNS with nanoparticle diameter of $d = 2.0\sigma$, and Figure 6c shows the phase diagram for h8t8 surfactant (modeled systems are inset in Figure 6). By examining the overall behavior presented in Figure 6, it is clear that comparing amphiphiles with similar linear length, namely comparing $d = 2.0\sigma$ TNS to the h2t8 surfactant, does not provide similar results. The h2t8 system more closely resembles Figure 1a, most notably exhibiting a PLH phase as well as an inverted hexagonally packed cylinder phase (IH), which is a natural progression as the headgroup gets increasingly forced into a structure with a curved interface due to the geometric constraints of the tail at high concentration. However, there are distinct similarities between the $d = 2.0\sigma$ TNS and h8t8 surfactant with respect to the phases observed and their concentration ranges. Instead of matching linear length, the excluded volumes of headgroups and tail groups of these systems are identical. In the same theme as the Israelachvili packing factor, where tail volume is related to headgroup area, a dimensionless volume can be constructed that relates the

(47) Schultz, A. J.; Hall, C. K.; Genzer, J. *J. Chem. Phys.* **2002**, *117*, 10329−10338.
(48) Horsch, M. A.; Zhang, Z.-L.; Iacovella, C. R.; Glotzer, S. C. *J. Chem. Phys.* **2004**, *121*, 11455−11462.
(49) Imai, M.; Kawaguchi, A.; Saeki, A.; Nakaya, K.; Kato, T.; Ito, K.; Amemiya, Y. *Phys. Rev. E* **2000**, *62*, 6865−6874.
(50) Schulz, M. F.; Khandpur, A. K.; Bates, F. S.; Almdal, K.; Mortensen, K.; Hajduk, D. A.; Gruner, S. M. *Macromolecules* **1996**, *29*, 2857−2867.
(51) Leibler, L. *Macromolecules* **1980**, *13*, 1602−1617.
(52) Israelachvili, J. N. *Intermolecular and Surface Forces*; Academic: London, 1992.
(53) Prinsen, P.; Warren, P. B.; Michels, M. A. J. *Phys. Rev. Lett.* **2002**, *89*.

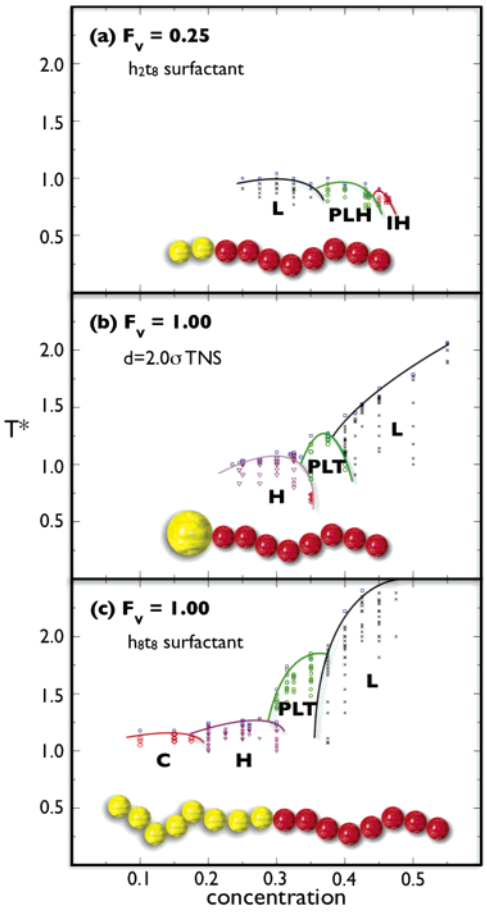

Figure 6. Temperature vs concentration phase diagrams for surfactant and TNS systems, with the schematics of modeled systems in inset. Phases are defined as lamellae (L), perforated lamellae through the headgroup (PLH), hexagonally packed cylinders (H), perforated lamellae through tethers (PLT), cubic ordered spherical micelles (C), and inverted hexagonally packed cylinders (IH). (a) Phase diagram for h2t8 surfactant system. (b) Phase diagram for TNS with particle diameter of $d = 2.0\sigma$. (c) Phase diagram for h8t8 surfactant system. In (a−c), the phase boundaries are approximate and drawn as guides for the eye.

volume of the headgroup to the volume of the tether. We therefore propose and use the following definition:

$$F_v = (\text{excluded volume of the head})/(\text{excluded volume of the tail}) \quad (7)$$

For both the $d = 2.0\sigma$ TNS and h8t8 systems, $F_v = 1.0$, whereas the dissimilar h2t8 system has a value of $F_v = 0.25$. Examining the phase diagrams presented in Figure 6 for the flexible surfactant, we again see the same trends with F_v as with 1/S, since small headgroups result in a small value of F_v, and F_v is large for large headgroups. Applying F_v to systems studied by Larson[33] and surfactants studied in Figure 6a,c, we see good agreement in the trends and phase diagrams between both TNS systems and surfactants. Thus the quantity F_v allows a direct, albeit rough, comparison between computational studies of coarse-grained surfactants and TNS models.

The geometric packing of the nanoparticle headgroups of the monotethered nanosphere model cannot be captured by standard surfactant models, which treat the headgroup as a flexible chain. However, there are additional entropic differences that also arise as a result of the headgroup treatment. This can be seen by comparing the $d = 2.0\sigma$ TNS and h8t8 phase diagrams. We observed that the TNS

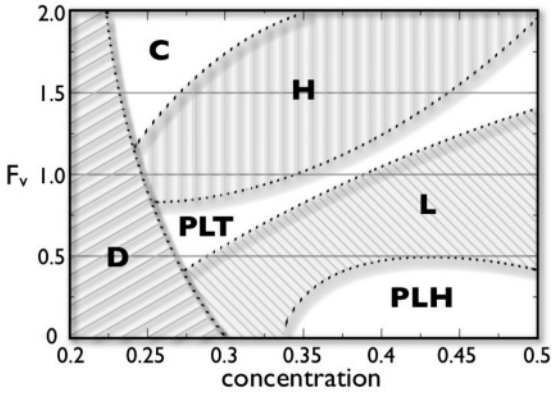

Figure 7. F_v vs concentration "phase diagram" for $T^* = 1.0$ for TNS. Phases are defined as lamellae (L), perforated lamellae through the headgroup (PLH), hexagonally packed cylinders (H), perforated lamellae through tethers (PLT), cubic ordered spherical micelles (C), and disordered (D).

model does not exhibit a cubic ordered micelle phase at low concentration, as did the surfactant model. This can most closely be attributed to the increased configurational entropy associated with the bead-spring model of the headgroup in surfactants. That is, the headgroup of the flexible surfactant has greater entropy, and a larger effective volume, as compared to the headgroup of the TNS with equivalent excluded volume. This can be illustrated by looking at the theoretical radius of gyration for a freely jointed chain in comparison to the radius of the TNS particle. For a freely jointed chain,[54] $R_g = \sqrt{N_{bonds}}L_{bond}/\sqrt{6} = 1.08$, as compared to $R = 1.0$ for the TNS; when the values are cubed to give relative volumes the differences can become rather significant, specifically the volume ratio of surfactant headgroup/TNS headgroup is 1.26/1.00. F_v attains the value 1.26 for the surfactant when utilizing the radius of gyration in calculating the headgroup volume. At lower concentrations, this slightly increased volume manifests itself in the stabilization of additional phases, therefore, direct comparisons between phases of surfactants and TNS may not be applicable at low concentrations. At higher concentrations, this increased volume does not manifest itself as additional phases, but rather as an increase in the order−disorder transition temperature, as is also seen when nanoparticle diameter is increased.

III.7. F_v versus Concentration Phase Diagram. We can additionally utilize F_v to more explicitly show the impact of nanoparticle size on the concentration dependent phase behavior. We can construct a diagram of F_v versus concentration, as shown in Figure 7, that unifies the previously plotted temperature versus concentration phase diagrams for different nanoparticle diameters. This diagram does not include order−disorder transitions as a function of temperature, but for temperatures below the order−disorder transition temperature, it may be used as a guide to the types of structures that might form and their relationship to each other.

IV. Conclusions

We predict that mono-tethered nanospheres form phases that strongly resemble the phases observed in surfactant systems. For certain nanoparticle diameters, concentration, and temperature, we observe the formation of cubic micelles, hexagonal cylinders, lamellar sheets, and perforated lamellar sheets. We demonstrate that for

(54) Larson, R. G. *The Structure and Rheology of Complex Fluids*; Oxford University Press: New York, 1999.

small nanoparticles relative to tether size the equilibrium structures favor sheetlike morphologies and for nanoparticles that are as large or larger than the tethers, curved morphologies are favored. We present a temperature vs concentration phase diagram for a three-dimensional system of TNS and a dimensionless scaling factor F_v that relates the size of the headgroup to that of the tether. F_v provides a mapping that may be useful when comparing between amphiphiles consisting of flexible chains to those containing a rigid and a flexible component. By mapping F_v vs concentration, it is possible to ascertain the stable morphology for either a flexible surfactant or a TNS. Finally, in contrast to the flexible surfactants, we observe an increase in the local geometric ordering of the nanoparticle as the size of the particle increases or as the concentration increases for a TNS tending toward local hexagonal packing at high concentrations.

Acknowledgment. Financial support was provided by the Department of Energy, grant no. DE-FG02-02ER46000. We thank the University of Michigan Center for Advanced Computing for CPU time. We are grateful to Ronald G. Larson and Elaine R. Chan for useful discussions.

LA051035L